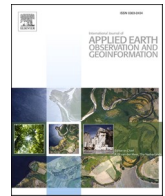


Contents lists available at [ScienceDirect](https://www.sciencedirect.com)

International Journal of Applied Earth Observations and Geoinformation

journal homepage: www.elsevier.com/locate/jag

New insights into the 2020 Sardoba dam failure in Uzbekistan from Earth observation

Ruya Xiao^{a,b,*}, Mi Jiang^c, Zhenhong Li^{d,e,f}, Xiufeng He^a^a School of Earth Sciences and Engineering, Hohai University, Nanjing 211100, China^b Key Lab of Reservoir Dam Safety, Ministry of Water Resources, Nanjing 210029, China^c School of Geospatial Engineering and Science, Sun Yat-sen University, Guangzhou 510275, China^d College of Geological Engineering and Geomatics, Chang'an University, Xi'an 710054, China^e Big Data Center for Geosciences and Satellites (BDCGS), Chang'an University, Xi'an 710054, China^f Key Laboratory of Western China's Mineral Resource and Geological Engineering, Ministry of Education, Xi'an 710054, China

ARTICLE INFO

Keywords:

Sardoba dam failure
2D displacements
Time-series InSAR
Internal erosion
Human factor of ignorance
Earth observation

ABSTRACT

On 1 May 2020, the Sardoba Reservoir in Uzbekistan breached its western wall, and the uncontrolled release of water caused casualties, environmental damages and economic losses. We investigate the dam failure based on three sets of Earth observation data, including: (i) satellite altimetry products, i.e., ICESat-2 data, with the aim of understanding the topographic features in the study area; (ii) multi-geometry Sentinel-1 SAR data to retrieve the pre-failure deformation along the vertical and horizontal east-west directions between 2017 and 2020; (iii) optical images from Sentinel-2 satellites and Global Precipitation Measurement (GPM) products, which are involved in exploring the environmental status before the failure. We analyse the possible causes of the collapse in terms of both physical and human factors. The differential settlement of ~60 mm revealed by InSAR at the failure section is a sign of internal erosion through the embankment, which is the physical factor contributing to the failure. The opportunity to prevent the collapse were missed due to the human factor of ignorance brought by limitations of the conventional monitoring methods. Neither ground observations nor satellite-based GPM products show extreme precipitation in the region, ruling out the likelihood of rainfall-induced overtopping. The settlement rate of the embankment shows no decaying trend, indicating that the dam is undergoing the primary consolidation phase of total settlement. Maximum settlement of ~270 mm (~0.8% of the dam height) has happened on the north bank since the reservoir impoundment, which should raise concern in future monitoring and surveillance. The results reveal that InSAR can discern the failure precursor by detecting surface motion, and that the deformation signals can help to warn of risks and avoid dam damage. We recommend InSAR deformation monitoring be included in future safety programs, providing detailed deformation and resisting risks of ignorance.

1. Introduction

Dams are barriers that restrict the natural flow of water. They create reservoirs that could suppress floods, and/or generate power, provide water for human activities such as agriculture, industry and municipal uses. While benefitting mankind, the dams have adverse effects on downstream communities, including the impacts on the safety of lives, the environment and properties. Dam accidents or failures could result in uncontrolled water release, hence, immense damage and loss of life. On 1 May 2020 (around 06:00 local time), a part of the Sardoba Reservoir dam in the Sirdaryo region of Uzbekistan failed. The extensive

flooding caused six deaths, huge environmental damages and economic losses. More than 100,000 people from Uzbekistan and neighbouring Kazakhstan had to be evacuated from their residences ([The Economist, 2020](https://www.economist.com/news/asia/2020/05/20/uzbekistan-dam-collapse)). Unfortunately, such tragedies have been common worldwide in recent years, for example, the May 2020 Michigan dam failures in the United States, the July 2019 Tiware dam breach in India, the August 2018 Swar Chung dam collapse in Myanmar, and the July 2018 Laos dam break.

Nowadays, there are still a large number of dams in operation, being planned or under construction around the world because of the demand of development. Keeping the dams well functioned and safe over their

* Corresponding author.

E-mail address: ruya.xiao@hhu.edu.cn (R. Xiao).

<https://doi.org/10.1016/j.jag.2022.102705>

Received 15 July 2021; Received in revised form 12 January 2022; Accepted 27 January 2022

Available online 3 February 2022

0303-2434/© 2022 The Author(s).

Published by Elsevier B.V. This is an open access article under the CC BY-NC-ND license

(<http://creativecommons.org/licenses/by-nc-nd/4.0/>).

entire lifespan is a challenging and never-ending task. For examples, the American Society of Civil Engineers (ASCE) scores dams a “D” in the 2017 Report Card for America’s Infrastructure; as of 2015, nearly 15,500 dams in the US are labelled as “high” hazard potential, while other 11,882 are classified as “significant” hazard potential (ASCE, 2017); China has more than 98,000 reservoirs of various dam types (Ministry of Water Resources P.R.China and National Bureau of Statistics P.R.China, 2013), and at the peak, at least one third of them are at-risk status (Zhang et al., 2014); between 1954 and 2014, there were 3,529 dam incidents in China (Zhang et al., 2017). An in-depth understanding of the damage characteristics of dam failures is essential to mitigate potential risks in the future.

The operational behaviour of the dam could hardly be obtained directly and can only be reflected by measurements of the deformation, total stress, leakage, etc. The dam safety relies on the advancements in monitoring and inspection techniques. Spaceborne Synthetic Aperture Radar Interferometry (SAR, InSAR) technique provides a new space geodetic means for deformation monitoring of the Earth’s surface (Biggs and Wright, 2020; Cigna and Tapete, 2021a, 2021b; Haghshenas Haghighi and Motagh, 2019; Lu et al., 2014; Wang et al., 2018) and infrastructures (Chang and Hanssen, 2014; D’Amico et al., 2020; Wu et al., 2020). Unlike conventional pointwise in-situ observation methods, such as levelling and Global Navigation Satellite System (Xi et al., 2018; Xiao et al., 2019), InSAR could provide dense observations at large spatial scales over long periods of time, enabling a more comprehensive analysis of dam deformation characteristics.

InSAR has been widely applied to monitor the deformation of several types of dams, such as gravity dams (Fornós et al., 2017; Wang et al., 2011), arch-gravity dams (Jiang, 2020; Milillo et al., 2016b), embankment dams (Tomás et al., 2013; Wang et al., 2020; Xiao and He, 2019; Zhou et al., 2016), and tailings dams (Du et al., 2020; Grebby et al., 2021; Silva Rotta et al., 2020), as well as the reservoir slopes and/or the dam surrounding areas (Dini et al., 2020; Liu et al., 2013; Saleh et al., 2018). Wang et al. (2011) and Milillo et al. (2016b) retrieved the phase history of dams using time-series InSAR technique and analysed the impact factors related to the deformations. Martire et al. (2014) investigated the accuracy of InSAR measurements and reported a strong agreement between the settlement results obtained from InSAR and the traditional method (extensometers). Milillo et al. (2016a), Al-Husseinawi et al. (2018) and Hu et al. (2017) used high temporal resolution InSAR results to reveal the different dam displacement processes in different periods and investigated the causes of the deformation behaviour changes. Emadali et al. (2017) presented the potential of very high spatial resolution SAR images (TerraSAR SpotLight Mode, up to 1.1 m azimuth resolution) to finely describe dam deformation, although such SAR data is currently not always available.

Previous works has focused on monitoring the deformation of dams and the surrounding areas using InSAR, as a complement to the existing safety monitoring programs. However, the use of InSAR technique for investigating water reservoir dam failures is a research gap. European Space Agency’s Copernicus program provides unprecedented opportunities for continuous radar mapping of the Earth with enhanced revisit frequency, with the potential to understand pre-failure deformation and the interactions between kinematic structures within dams with sufficient resolution. In addition, InSAR’s unique ability to “turn back time” allows historical deformation to be analysed retrospectively, regardless of whether ground monitoring is carried out. There is no doubt that InSAR pre-failure deformation measurements will be an important source of data for post-event investigations. Herein we retrieve the vertical and horizontal pre-failure deformations of the Sardoba Reservoir dam (Uzbekistan) using satellite remote sensing data. The historical displacement time series covering the period from the construction completion to the failure event can help gain insight into operational behaviours and investigate possible factors leading to the failure. To our knowledge, this is the first application of InSAR in the investigation of a catastrophic water reservoir dam failure.

The paper is structured as follows: Section 2 describes the study area and Section 3 gives a brief overview of the SAR data involved and the methods used for InSAR processing. Section 4 shows the InSAR Line-of-Sight (LOS) deformation and the horizontal and vertical displacements from multi-geometry. Section 5 discusses identifying what happened (the physical causes of the dam’s failure), why it happened (the human causes) and the lessons learned (avoiding such failures from happening again). Finally, concluding remarks are drawn in Section 6.

2. Study area

The Sardoba Reservoir, located in the eastern region of Sirdaryo, Uzbekistan, was fully completed in 2017 after seven years of construction. With a maximum water storage capacity of ~ 920 million m^3 , the reservoir serves for agricultural irrigation in the Sirdaryo and Jizzakh regions. Water is diverted from the Syr Darya (Syr River) through a network of canals and impounded into the reservoir. Fig. 1a shows the location of the Sardoba Reservoir and the neighbouring topography. The Sardoba Reservoir is a plain reservoir, the area around which is flat. The terrain is one of the reasons why uncontrolled floods spread rapidly and affect a wide area after the dam burst. Optical and SAR intensity images before and after the 1 May dam failure are shown in Fig. 1b–1e. We can see that the north, east and west sides of the reservoir are surrounded by embankment dams (earth and rockfill) with a total length of more than 27 km, and the south part of the Sardoba Reservoir is an open area. The area of water in the reservoir at capacity is more than 50 km^2 . Satellite images before the dam breach suggest the reservoir was operating at a high water level, even close to full capacity. From the images captured after the failure, the length of the dam collapse is estimated to be ~ 250 m.

To better understand the topographic features, we accessed NASA’s Ice, Cloud and land Elevation Satellite-2 (ICESat-2) L3A Land and Vegetation Height products (Neuenschwander et al., 2019) for the elevation profiles covering the study area (Fig. 2). The along-track height data for the ground surface were acquired by the Advanced Topographic Laser Altimeter System (ATLAS) onboard ICESat-2. As shown in Fig. 2a, ground elevation of the study area in the south is higher than that in the north. Thus, compared to the northern part of the reservoir, the southern part is a shallow area. Some photons of track GT2L return from the dam surface and form a peak on the height profile plot in Fig. 2b. The height difference between the dam top and the ground surface to the north of reservoir is estimated to be ~ 30 m. Consistent with the information disclosed by the media, the highest point of the dam is ~ 32 m (on the north side of the reservoir) and the height of the lowest point is ~ 28 m (the southern sections on the east and west sides of the reservoir dam).

The Sardoba reservoir was constructed in phases and zones until 2017. Exploration through Google Earth™ historical imagery revealed that the northernmost zones of the reservoir began to store water as early as 2014. Weirs are used for zoning water storage, so that only a portion of the reservoir held water when the stock is low. This explains why water remained in the northern part of the reservoir a few days after the dam failure, but was drained in the southern part (Fig. 1c and 1e). When the Sardoba Reservoir is fully operational, the storage capacity is scheduled to meet the demands for different periods. Fig. 3 display remote sensing images of the water in the Sardoba Reservoir, and we note significant changes over the course of a year (from May 2019 to April 2020). The reservoir was almost at capacity in May 2019, and from July onwards the water area began to decrease, indicating that the water level was dropping and a large amount of water was being discharged. The stock reached its lowest in October. The Sentinel-2 optical image captured on 2019-10-22 depicts the southern part of the reservoir had been drained, and the reservoir bed was dried out. A new round of water storage in the reservoir started in November 2019. The water area gradually expanded, reaching the maximum in March 2020, and remained at the peak until the dam broke on 1 May.

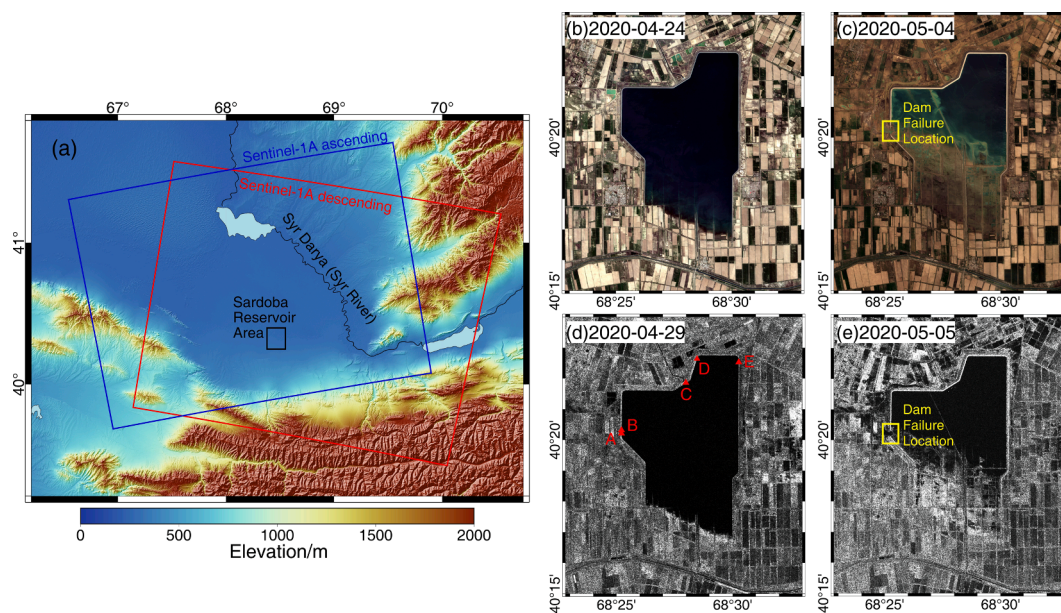


Fig. 1. Overall study area. (a) Location of the Sardoba Reservoir with topography as the background map, and the coverage of Sentinel-1 data used. (b) and (c) are optical remote sensing images from Sentinel-2 satellite (natural colour band combination of red B4, green B3, and blue B2) acquired before (on 2020-04-24) and after (on 2020-05-04) the dam failure, respectively. (d) and (e) are SAR intensity maps from Sentinel-1 acquired on 2020-04-29 and 2020-05-05, respectively. The rectangles in (c) and (e) indicate the location of the failure section on the dam.

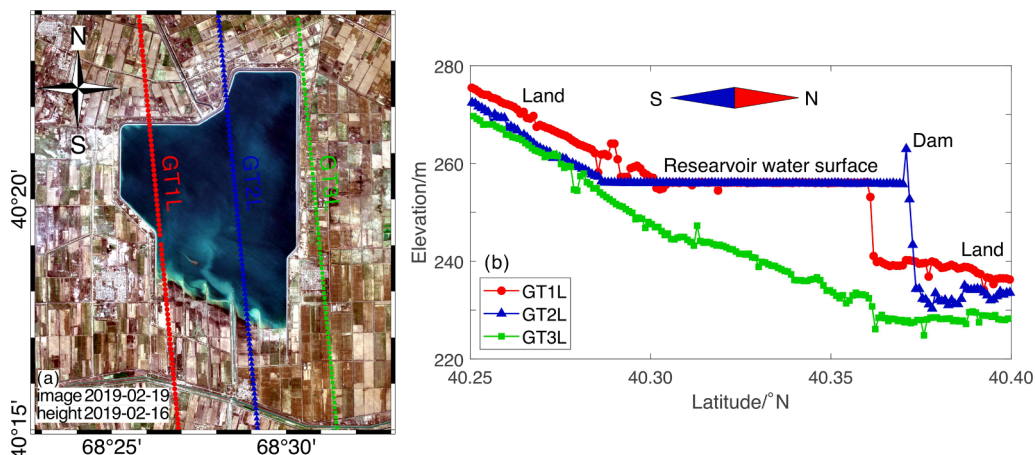


Fig. 2. Along-track height profiles of the study area from ICESat-2 ATLAS. (a) Footprint of the three laser beams (ground track [x] left, G.T. [x]L) of the ICESat-2 ATLAS. The optical image is from the Sentinel-2 satellite on 2019-02-19, and the ATL08 product is acquired on 2019-02-16. (b) Elevations above the WGS84 ellipsoid for the three profiles.

3. Multi-temporal InSAR processing

3.1. Time-series InSAR analysis

We exploit 145 Sentinel-1A SAR images acquired during 2017–2020 after construction, including 75 images in ascending track with a heading angle of 346.5° and incidence angle of 39.5° , and 70 images in descending track with a heading angle of 193.5° and incidence angle of 40.4° . Because vegetation and agricultural land cover dominate the surface features in the Sirdaryo area, the performance of InSAR is challenged by the fast decorrelation which occurs over a short period. Hence, only interferometric pairs with a temporal baseline of less than 60 days are selected to enhance coherence in the following time-series analysis. The numbers of interferograms used in ascending and descending tracks are 360 and 317, respectively. The spatial and temporal baselines of the interferograms are shown in Fig. 4.

During the TOPS (Terrain Observation by Progressive Scans) SAR co-

registration, we first applied a 30 m resolution SRTM DEM (Digital Elevation Model) and Sentinels Precise Orbit Determination service to conduct the geometry co-registration for each burst interferogram. A network-based Enhanced Spectral Diversity approach emphasising the maximisation of coherence was used to estimate time-series azimuth shifts (Jiang, 2020). After resampling all co-registered SAR images to a common reference geometry, the differential interferogram series are obtained in single look. To retrieve the temporal behaviour of the dam pre-failure motion, we carried out time-series InSAR analysis in the StaMPS/MTI framework with some improved strategies. The flowchart of the data processing is shown in Fig. 5.

We employed phase stability analysis to identify candidates for coherent pixels (Hooper et al., 2007). Targets with an amplitude dispersion of less than 0.4 were first selected (Ferretti et al., 2001), and then, all spatially correlated phase components on these targets were removed by low-pass filtering and Fast Fourier Transform fringe rate estimation (Hooper et al., 2007). Candidates were finally confirmed by

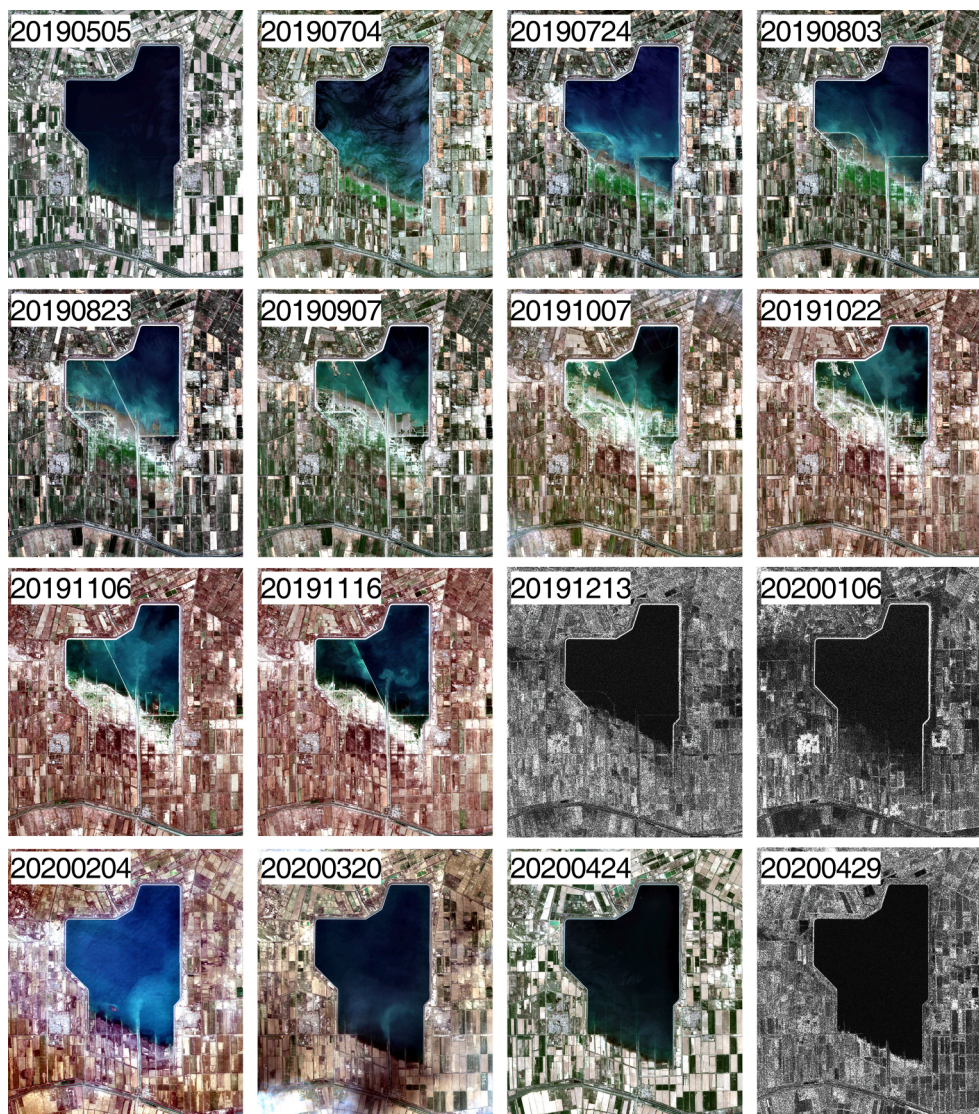


Fig. 3. Remote sensing images show the water area changes in the Sardoba Reservoir from May 2019 to April 2020. The optical images in colour are from Sentinel-2 satellites, and the SAR images in grey (dated 2019-12-13, 2020-01-06 and 2020-04-29) are from Sentinel-1 satellites.

thresholding temporal standard deviation of less than 0.8 rad. Because of the low phase gradients over this low-coherence scenario, all coherent targets were resampled into a grid to enhance smoothness. The integer phase ambiguity of each interferogram was estimated by the SNAPHU unwrapping method (Chen and Zebker, 2002), followed by a phase unwrapping correction algorithm. We corrected unwrapping errors by automatically testing the unwrapped phase loops in the temporal network in Fig. 4. The Lasso regularisation method was used to calculate the integers for compensation (Xu and Sandwell, 2020). The corrected integer phase ambiguities together with the wrapped phases compose the unwrapped phase series with full resolution. Based on the unwrapped phases, we used least squares to remove topographic errors by analysing the time-series unwrapped phase to the perpendicular baseline.

3.2. Determining two-dimensional displacements

What InSAR measures are the projections of the ground target's movements to the satellite LOS direction. From the geometry shown in Fig. 6, we can get the relationship between the LOS deformation, D_{los} , and three-dimensional components as (Wright et al., 2004):

$$D_{los} = (\sin\theta\sin\alpha, -\sin\theta\cos\alpha, \cos\theta) \begin{pmatrix} d_{NS} \\ d_{EW} \\ d_{UD} \end{pmatrix} \quad (1)$$

where θ is the incidence angle, α is the heading angle (clockwise from the north direction), and $(d_{NS}, d_{EW}, d_{UD})^T$ are the three-dimensional (North-South, East-West and Up-Down) components of the deformation.

Theoretically, the three-dimensional (3D) motion could be resolved with multi-geometry (three or more) observations. Since SAR satellites travel in Sun-synchronous orbits, the N-S motion component is hard to be separated accurately due to poor geometric constraints. LOS deformation is less sensitive to the displacement in the N-S direction than those in the E-W and U-D directions. For example, in this case, the projection vector component coefficients of the ascending geometry are -0.15 , -0.62 and 0.77 for the N-S, E-W and U-D directions, respectively. The contribution from the N-S is the smallest of the three directions. Fuhrmann and Garthwaite (2019) reported that the condition number of the coefficient matrix, which represents a measure of the sensitivity of the linear system solution to data errors, improved 10 times when neglecting movement in the N-S direction. They suggested that the resulting errors are acceptable with regards to the general noise level of

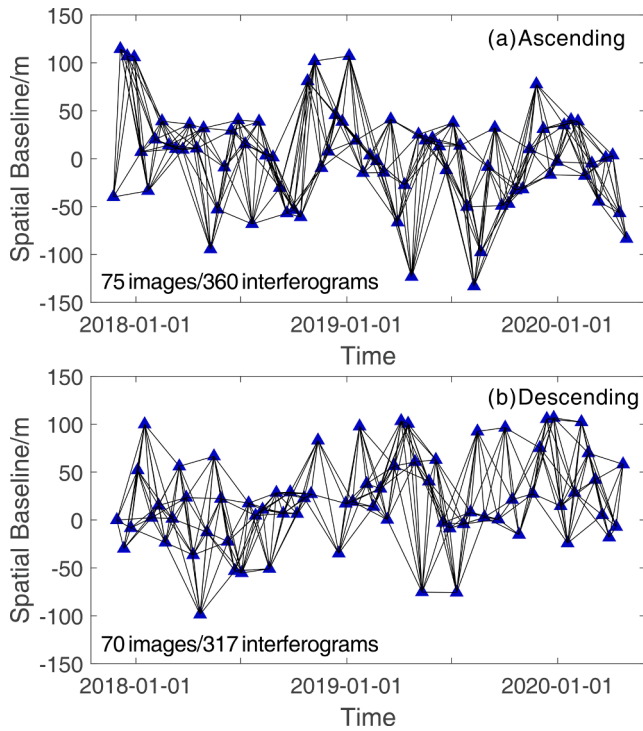


Fig. 4. Temporal and spatial baselines of the interferograms.

InSAR measurements. When omitting the N-S component of deformation, the vertical U-D and horizontal E-W displacements can be estimated from the ascending and descending satellite geometries:

$$\begin{pmatrix} d_{EW} \\ d_{UD} \end{pmatrix} = \begin{pmatrix} -\sin\theta_{asc}\cos\alpha_{asc} & \cos\theta_{asc} \\ -\sin\theta_{des}\cos\alpha_{des} & \cos\theta_{des} \end{pmatrix}^{-1} \begin{pmatrix} D_{asc} \\ D_{des} \end{pmatrix} \quad (2)$$

where θ_{asc} and θ_{des} are the incidence angles, α_{asc} and α_{des} for the heading angles, and D_{asc} and D_{des} are LOS deformations observed from the ascending and descending tracks, respectively. This 2D displacement function model is especially suitable for the east and west sides of the embankment dam in this case, where we consider that little movement occurs in the N-S direction.

4. Results and analyses

4.1. Full-resolution LOS deformation

About 130,000 coherent pixels are selected in the study area. It is clear from Fig. 7 that measurement points are denser on the crest and the upstream surface of the Sardoba Reservoir dam due to the asphalt or concrete paving, ensuring better coherence. The LOS displacement rates in Fig. 7 shows that the Sardoba Reservoir dam deformed during the study period, while the surrounding agricultural land remained stable.

Due to the different imaging geometries, the displacements observed from the ascending and descending satellite tracks present different patterns. For example, the east side of the embankment dam shows obvious deformation in the ascending track (Fig. 7a), while being relatively stable in the descending map (Fig. 7b). This is because, besides settlement, the dam is also experiencing horizontal displacement. The loads acting on the Sardoba Reservoir dam includes self-weight, water level oscillation and seepage pressure, etc. Deformation is the response to the acting loads and is mostly due to the materials adjusting to stress distribution.

Fig. 8 presents a demonstration model to show the geometry between the InSAR LOS observations and dam's motions. The horizontal (E-W)

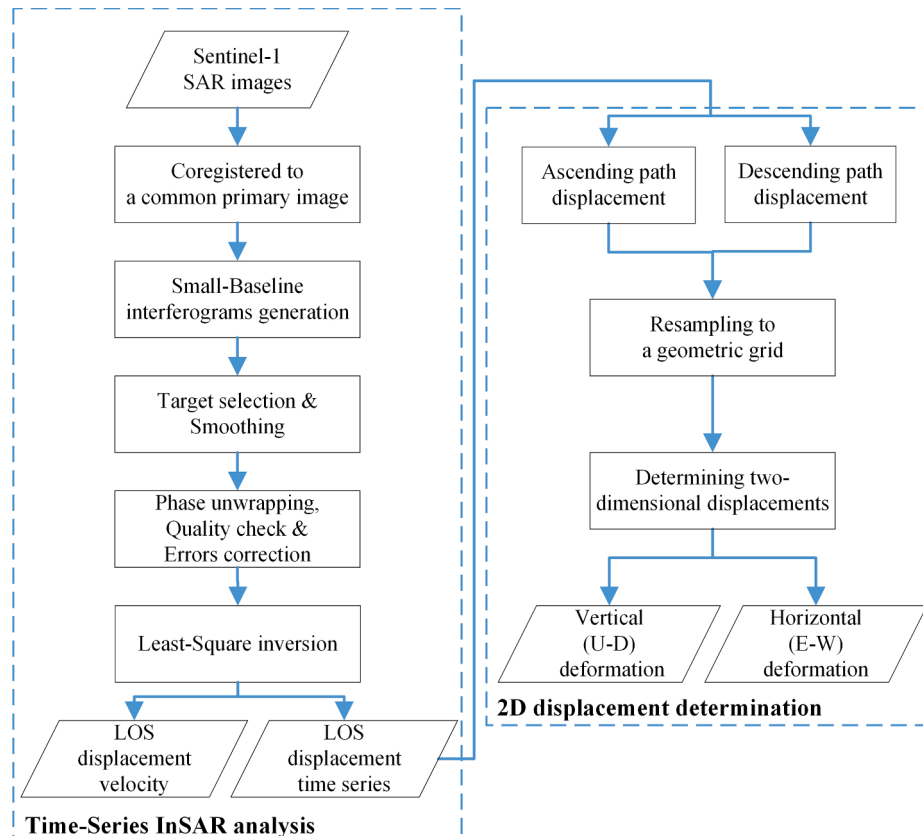


Fig. 5. Flowchart of the InSAR data processing.

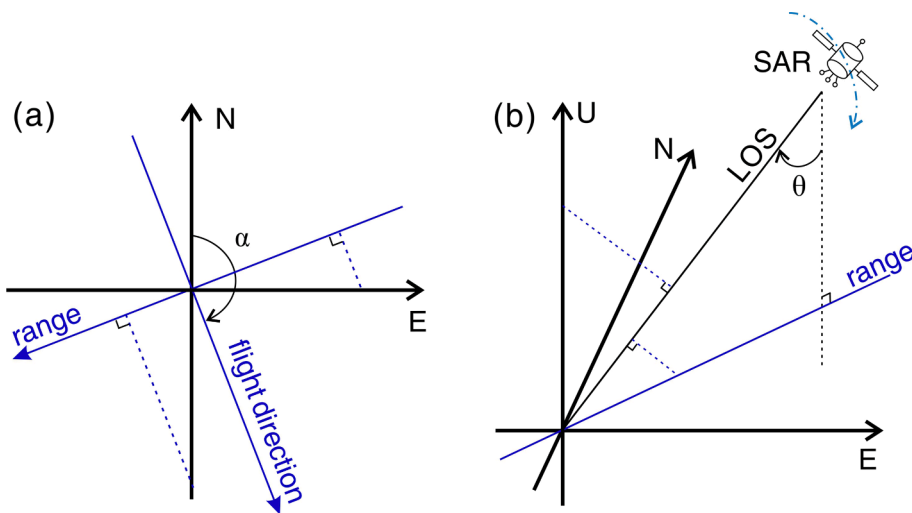


Fig. 6. (a) The displacement projection geometry in the N-E plane. (b) Three-dimensional view of the projection geometry.

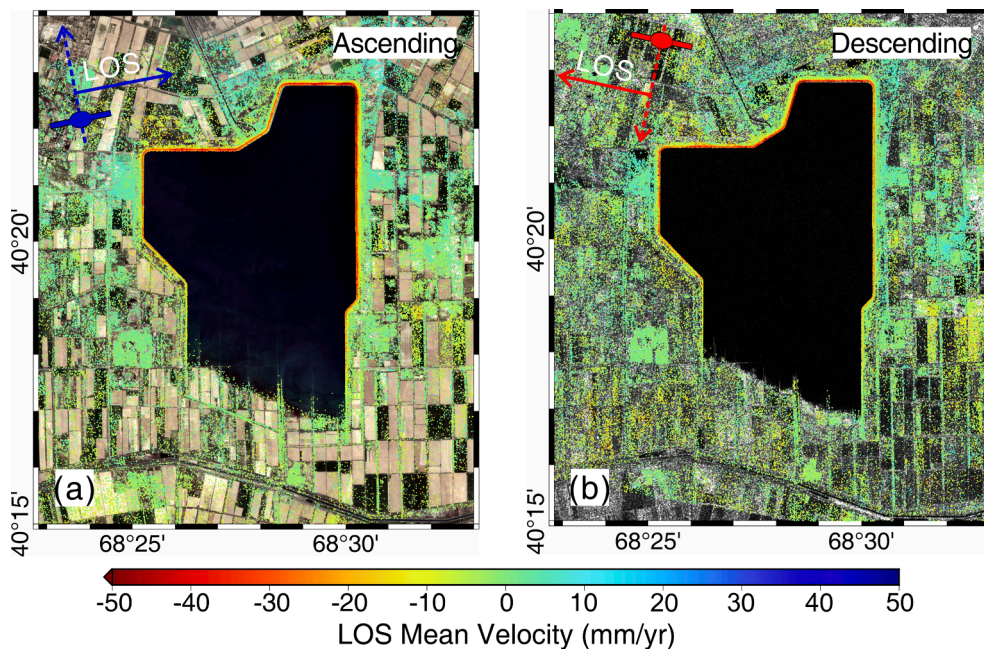


Fig. 7. LOS displacement rate observed by the ascending and descending geometries. A negative value means motion away from the satellite.

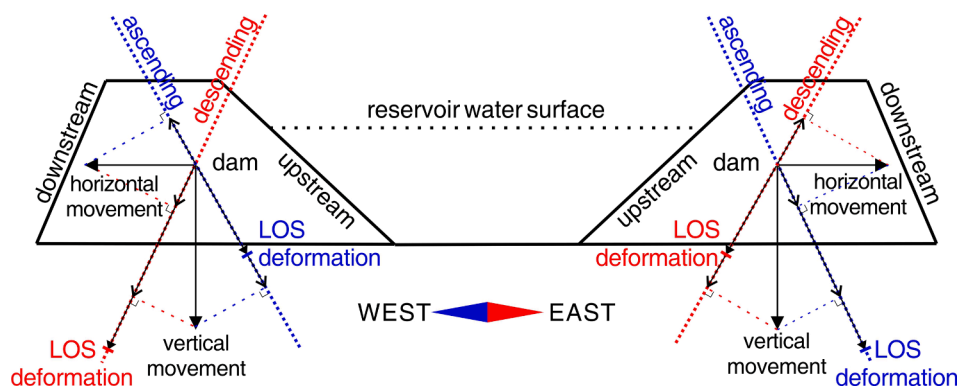


Fig. 8. A diagram shows the geometries between InSAR LOS observations and dam motions.

and vertical movements of the dam are projected onto the satellite ascending and descending LOS directions. As the embankment moves eastwards and downwards, the deformation magnitude in the ascending track is larger than that in the descending track. That is because the deformation components cancel each other out when projected to the descending track. A single geometric observation does not provide accurate measurements and may lead to misinterpretation of the dam's deformation pattern, as the LOS displacement may differ noticeably from the real motion. This explains the difference in deformation observed by SAR instruments with different look angles and why we need to combine the ascending and descending images to reveal more accurate dam motions.

4.2. Gridded two-dimensional deformation

To increase the identical observations from both ascending and descending satellite orbits, we established a regular grid of $15 \times 15 \text{ m}^2$ per cell size in the geographic coordinate system, and down-sampled the full-resolution deformation fields into it. Linear temporal interpolation was applied to obtain the "complete" displacement time series on each imaging date. Fig. 9 presents the horizontal and vertical displacement rates for over 21,900 targets. Although less dense than full-resolution observation, it still provides better spatial details than any other conventional terrestrial surveying method (e.g., levelling, GNSS and total station surveying), and can reveal deformation pattern of the dam with sufficient resolution.

4.2.1. Horizontal displacement rate

The directions of the horizontal displacement vary at the different parts of the Sardoba Reservoir dam. The north bank (near location D shown in Fig. 1d) tends to move westward, while the northeast section (near location E) of the embankment dam deforms downstream. Only slight displacement rates are observed at the south dam sections of the east and west banks of the reservoir. This is because various sections of the dam are experiencing different internal and external conditions. As a rule of thumb, the crest of a dam deforms slightly upstream during the first filling of the reservoir and then moves downstream as the phreatic surface develops within the embankment (Fell et al., 2015). From the archived remote sensing images, two rounds of water evacuation and

filling happened in the Sardoba Reservoir, one of which is shown in Fig. 3. Therefore, the south sections of the dam underwent two "first fillings". Also, the external loads from the reservoir at the south sections are smaller due to the shallow water. To a certain extent, these may have contributed to the insignificant horizontal displacement in the south dam sections.

Generally, the magnitude of horizontal dam deformation is less compared to the vertical direction. For a well designed and constructed dam, it is commonly considered that the horizontal deformation will be within an acceptable limit when the vertical deformation amplitude is within a safe range (U.S. Department of the Interior Bureau of Reclamation, 2011). Engineers are more concerned with vertical settlement in practice.

4.2.2. Vertical settlement rate

Settlement is an inevitable natural process for earth and rockfill embankment dams. The deformation rate of the dam helps to determine whether the settling process of the embankment is decaying and whether the settlement is normal or unusual. In this paper, we focus on the period from the completion of the dam project to the dam failure, i. e., late 2017 to May 2020, which is a relatively short period compared to the consolidation processes of the dam materials and the designed dam lifespan. Fig. 9b shows that settlement occurs mainly on the crest or the upstream face of the Sardoba Reservoir dam, with the toe of the dam behaving steadily. Due to the limitations of SAR resolution and imaging mechanism, it is difficult to confirm the exact location of the scatterer. Therefore, we cannot tell the specific height of the dam where the deformation takes place, e.g., whether subsidence happens at the crest or the middle of the dam slope.

The spatial deformation patterns of the Sardoba Reservoir dam show that the northern part (including the north bank and the northern region on the east and west banks) settles faster than the southern part. The largest subsidence is observed on the north bank, with a maximum rate of over 50 mm/yr. Smallest settlements are found on the southern part of the east bank, whose displacement rate is less than 10 mm/yr. The spatial difference in settlements of the two regions may be attributed to two factors: (i) higher dam height of the northern dam part than the southern as the ground elevation in the area gradually decreases from south to north; and (ii) deeper reservoir water in the north, which causes

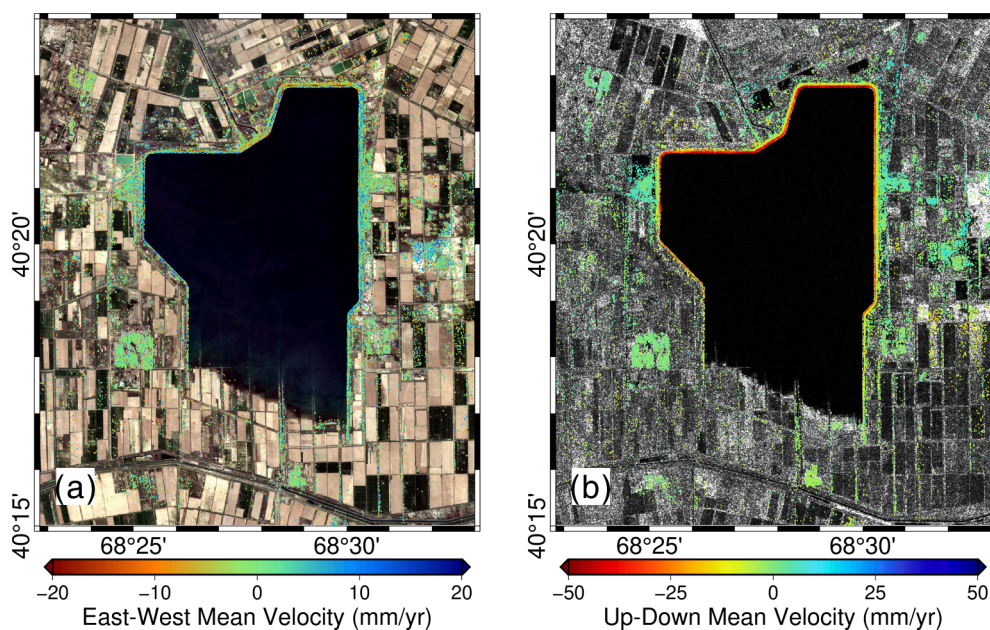


Fig. 9. (a) The mean horizontal East-West displacement velocity map, with the positive values implying eastward motion. (b) The mean vertical Up-Down displacement velocity map, with the negative values indicating settlement.

greater external pressure on the northern sections of the embankment.

4.3. Displacement time series

The cumulative displacement is another important parameter of interest. To better understand the kinematic behaviour of the embankment dam, we plot the deformation time series for five selected sites (Location A - E shown in Fig. 1d) as shown in Fig. 10. The first column shows the LOS time-series displacements obtained from the ascending and descending geometries, and the second column displays the derived 2D time-series displacements.

Site A is located within the dam failure section, and B is on the embankment to the north of the break. The deformation time series (Fig. 10a1 and 10a2 vs Fig. 10b1 and 10b2) exhibit similar characteristics but of different magnitudes. Both sites experienced eastward horizontal motions and the cumulative settlements at sites A and B

reached ~100 mm and ~40 mm, respectively. The differential settlement in this area is the physical cause of the dam failure on 1st May, which will be further discussed in Section 5.1.2.

Site C is close to the outlet works of the Sardoba Reservoir. Since the conduits of the outlet works are constructed through the embankment, differential deformations may occur at the joint. Relative movements could cause flow surface irregularities, giving rise to an erosion failure of the appurtenant structure. Therefore, deformation observations at this location play a primary role in ensuring the safety of the outlet structure. The horizontal displacement at site C is fluctuating slightly, and the net horizontal deformation is minimal, being less than 10 mm throughout the monitoring period (Fig. 10c2). Results indicate that the vertical motion dominates the dam crest area near the outlet works. The cumulative subsidence at site C reached more than 90 mm, equivalent to a settling rate of ~40 mm/yr.

The last two rows in Fig. 10 show two different deformation patterns.

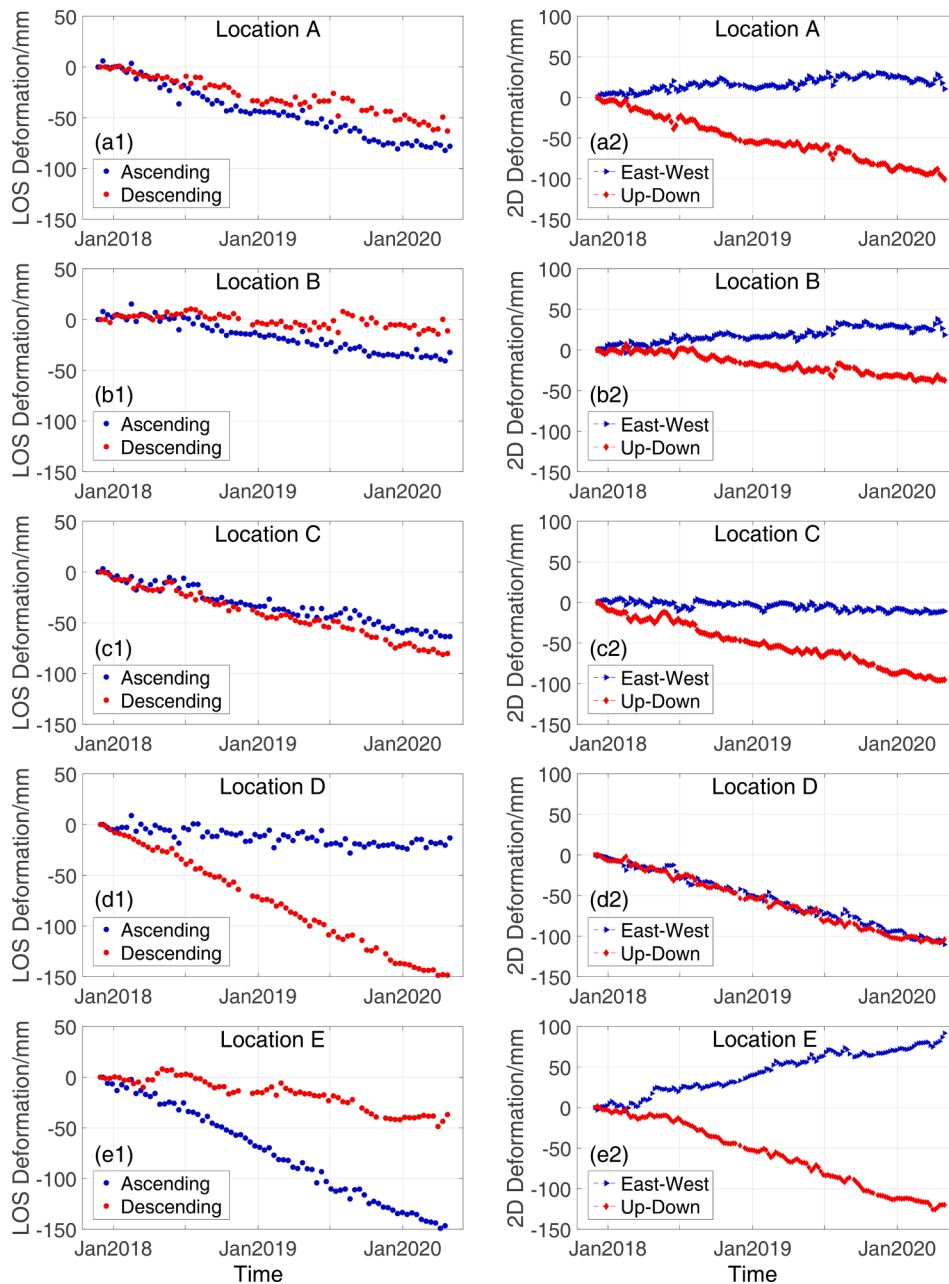


Fig. 10. Deformation time series and 2D (E-W horizontal and vertical) decompositions for selected sites A - E, whose locations are marked in Fig. 1d. The first column (a1 - e1) shows the ascending and descending LOS displacements; the second column (a2 - e2) presents the horizontal (E-W) and vertical displacements.

For site D, the magnitude of the cumulative deformation observed from the ascending path is relatively small, whereas that is large from the descending geometry. The situation for site E is the opposite (large for the ascending but small for the descending path). The opposite horizontal motion directions at these two sites (shown in Fig. 10d2 and 10e2) are responsible for the difference. From the 2D results, we can see the cumulative settlements of both locations exceed 100 mm. Site D moved ~100 mm to the west, while E experienced a motion of more than 90 mm to the east.

4.4. Analysis of dam deformation

The total embankment settlement consists of three components: the immediate settlement, the primary consolidation and the secondary consolidation. The implicit assumption here is that the soil grains and pore fluid themselves, as components of the two-phase material, are incompressible. The immediate settlement is regarded as an elastic process, although there may be plastic flows that lead to an underestimation of deformation magnitude. It occurs immediately in response to loading since the dam's construction. As we are acquiring post-construction deformation of the Sardoba Reservoir dam, the proportion of immediate settlement in the observed deformation is negligible. The primary consolidation deformation refers to the voids volume decrease as porewater is squeezed out of the soil. The dissipation of excess pore water pressure may last for a long time, depending upon the permeability of the soil. The secondary consolidation, also known as creep settlement, occurs when effective stress remains unchanged after the dissipation of a large proportion of excess pore pressure. Empirically, it takes years before the settlement enters the secondary consolidation phase. For example, the Spring Canyon Dam of the Horsetooth Reservoir in Colorado, US, is still experiencing the primary consolidation settlement 35 years after the completion of construction (U.S. Department of the Interior Bureau of Reclamation, 2011). The vertical deformation time series with relative constant slopes (Fig. 10) suggest that the Sardoba Reservoir dam has not achieved secondary consolidation.

During normal operations (static conditions), the deformations are influenced by the level and distribution of stresses within the embankment under three reservoir loading conditions, i.e., the first filling, normal operational cycling, and rapid drawdown. The pore pressure within the materials dissipates to a certain degree before the completion of construction, and the consolidation process dominates from the period close to dam construction completion to the first filling of the reservoir. When the reservoir is filled, wetting phenomenon causes the strength and rigidity of the material to decrease, resulting in saturation collapse. Seepage develops within the unsaturated materials and causes changes in pore pressure and effective stress, which leads to deformation. Fluctuations in reservoir level not only affect the external loads acting on the dam but also change the phreatic surface within the embankment. The consolidation may slow down or cease as the development of the phreatic surface, depending on the relative magnitude between residual pore pressures of construction and the steady seepage-induced pore pressures (U.S. Department of the Interior Bureau of Reclamation, 2011). For steady seepage conditions, the distribution of pore pressures is controlled by the flow net, which is a grid formed by the intersection of a set of streamlines and equipotential lines. Assuming the water level drops suddenly, the drainage of pore water in the soil voids cannot occur in time due to the low permeability of fill material. In that case, the steady seepage condition turns to the rapid drawdown condition. The stability of the upstream slope is critical, as the phreatic surface remains unchanged while the stabilising effect of water support no longer exists.

As the water level records of the Sardoba Reservoir are inaccessible, it is impossible to quantitatively analyse the relationship between the water level changes and dam settlement. Nevertheless, the waterbody area changes interpreted from the remote sensing images can roughly reveal the water level fluctuations. It is found that two rounds (filling,

evacuation, and refilling) of significant water level changes occur during the study period, one of which is shown in Fig. 3. However, the deformation time series for the five selected sites (Fig. 10) show quasi-linear subsidence, and none of them presents clear rhythm relevant to changes in water level. This suggests that consolidation governs the settlement of the Sardoba Reservoir dam, although the deformation is controlled by both the dissipation of excess pore water pressure and seepage pressure.

The major effects of deformation on the dam include the loss of freeboard and cracks. Freeboard is the vertical difference from the crest elevation of the embankment to the design of the maximum reservoir water surface, and it should be sufficient to prevent overtopping which may cause dam failure. In modern dam design and construction, there is a vertical distance between the design crest elevation and the constructed top of the dam to accommodate long-term consolidation, known as "camber". A rule of thumb of using 1% embankment height as the camber is a common practice (U.S. Department of the Interior Bureau of Reclamation, 1987), especially for the low dams (height less than 60 m). The deformation observed by InSAR can help engineers judge whether the magnitude of post-construction settlement of the Sardoba Reservoir dam is normal, and whether there is an adverse effect on the freeboard. The dam sections in the northern part of the reservoir were first completed and put into use (since 2014) and experienced the maximum settling rate. Based on an assumption of a relatively stable displacement rate after construction, it is estimated that from 2015 to April 2020, the vertical deformation on the north bank of Sardoba Reservoir could exceed 270 mm, which is about 0.8% of the dam height. This kind of dam deformation magnitude is not unusual, but worthy of operators' careful attention.

Differential settlement of dams during or after construction may form cracks below the reservoir level and result in uncontrolled seepage and initiation of internal erosion in the embankment. Therefore, in addition to the magnitude, the pattern of settlement is also crucial in safety monitoring. We have noticed that the deformations of the dam crest are not constant at different sections, which means uneven settlement occurs on the Sardoba Reservoir embankment. Without awareness and proper intervention, it could lead to catastrophic consequences, and we will discuss that further.

5. Discussion

Based on all the information retrieved by the Earth observations, a retrospective analysis of the Sardoba Reservoir dam failure is carried out and the possible failure mode and causes of the catastrophic event are investigated. Experience of water projects, Potential Failure Mode Analysis (PFMA), and the statistics of historic dam failures and incidents, are also considered. All the inferences and discussions are evidence-based to our best knowledge.

5.1. What happened: physical causes of Sardoba dam failure

5.1.1. Is rainfall a trigger factor?

Overtopping is one of the most commonly seen failure modes of dam collapses and is caused by the water spilling over the top. Historical statistics of embankment dam failures indicate that overtopping was responsible for about half of the failures where the mode of failure is known (Fell et al., 2015; Foster et al., 2000). According to the Association of State Dam Safety Officials (ASDSO) Dam Incident Database (ASDSO, 2020), overtopping accounts for ~34% of all dam failures in the US from 2010 to 2019. In many cases of dam failures, the water level rise in front of the embankment due to rainfall is one of the triggers, like the May 2020 Edenville and Sanford dam collapses in Mid-Michigan, US (BBC News, 2020). Heavy rains in the reservoir region and/or the upper zone of the runoff area lead to extreme floods and the consequent overtopping.

We note "a week of heavy rain" was mentioned in several media or study reports (CSSTEAP, 2020; NASA Earth Observatory, 2020),

suggesting that rainfall in the region is one of the trigger factors for the May 2020 Sardoba dam failure. Giri et al. (2020), in their preliminary analysis, suggest that the “overtopping due to extreme rainfall and wind wave” could be one of the possible causes of the failure.

However, we accessed five ground observations in the vicinity of the Sardoba Reservoir, as well as the Integrated Multi-satellite Retrievals for Global Precipitation Measurement (IMERG) data, and found that there is no heavy rain within the region in the past month. The precipitation for April 2020 is shown in Fig. 11. The five weather stations, with the World Meteorological Organization identifier 38581, 38583, 38584, 38579 and 38713, are at distances of approximate 44 km, 56 km, 59 km, 58 km and 63 km from the Sardoba Reservoir (data provided by the website “Reliable Prognosis”, https://rp5.ru/Weather_in_the_world). We used 1 Day IMERG Late Run precipitation accumulations (Huffman et al., 2020) of ~ 10 km spatial resolution and calculated a 50×50 km² average. Both ground and satellite datasets show no significant rainfall (daily precipitation > 10 mm) in the two weeks before the dam breach. Even throughout April, there were no extreme storms or intense rainfall in the region.

The Sardoba Reservoir, as a human-made project, is a regulation reservoir and does not collect water from natural runoff gathering. Its inflow almost comes from the Syr Darya through a network of canals and is scheduled manually. In the absence of extreme rainfall in the area, there was no additional incoming water resulting in an uncontrolled rise in water levels. Thus, we can rule out that the break is caused by overtopping as the dam does not have a significant loss of freeboard.

5.1.2. Differential settlement at failure section

In Figs. 9b, 10a and 10b, we note that the section of embankment dam near the breach location experienced differential settlements before the failure event. A close-up of the dam break section on the satellite image is shown in Fig. 12a, with seven measurement points marked. These selected measurement points derived from SBAS InSAR are all located on the crest of the embankment dam, with distances between adjacent positions less than 100 m. Fig. 12b represents the vertical settlement profile along the dam, where T3, T4 and A are within the dam failure section and T1, T2, B and T5 are not. The vertical deformation of the dam failure section before the burst is more significant than that of the non-failure section. On average, the dam break section (T3, T4 and A) settled by ~ 40 mm more than the non-failure section (T1, T2, B and T5) during the monitoring period. The maximum settlement occurred near location A and reached 100 mm from December 2017 to April 2020. The subsidence difference between A and B, with a distance of ~ 90 m, exceeded 60 mm, which approximates 0.2% of the dam height. From the Google Earth™ historical images, the dam breach section was put into use from the end of 2015. Upon reasonable speculation, the actual uneven settlement between 2015 and 2020 could reach twice the observed value from 2017 to 2020. Although the deformation pattern of the embankment is on a case-by-case basis, experience has shown that

zones with differential settlement greater than 0.5% of the dam height are most likely to suffer cracking and hydraulic fracture (Fell et al., 2015). It is wise to consider the differential settlement as an unusual deformation pattern and take proper interventions.

The time-series displacements of the selected locations are shown in Fig. 12c. As can be seen, the settlement difference between locations A and B increased to ~ 30 mm at the end of 2018 and further reached over 50 mm a year later. The deformation time series present more time-varying details besides the quasi-linear settlement trend. The vertical displacement rate at location A is greater in the second half of 2018 than in the first half of 2019, and the rate increased slightly in the latter half of the year. The net cumulative subsidence at location B is almost zero in the first half of 2018 and is relatively small in the first four months of 2020. There seems to be “abnormal deformations” in mid-2018 and mid-2019, which are most likely to be related to the water level changes in the reservoir. Remote sensing imagery shows that there were significant reductions in water area during the two periods, which imply reservoir drawdowns. When rapid drawdown occurs, pore pressure in the upstream zone and foundations of the embankment may not dissipate in time. In this condition, high pore pressure remains within the embankment, while the stabilizing effect of the water on the upstream face is no longer available. The deformations possibly suggest elastic responses of the dam surface to the pore pressure changes. Thanks to the short revisit period of spaceborne SAR (compared to traditional deformation measurement methods such as levelling), the deformation process can be revealed in more detail. These subtle differences in rates could be related to external pressure and seepage force changes caused by reservoir level fluctuations.

5.1.3. Most likely failure mode: internal erosion

Deformation of the embankment dam is expected to occur during construction and initial operation. However, adverse deformation or uneven settlement could lead to (or be due to) seepage-related internal erosion. Internal erosion refers to the process that seepage water flow takes away soil particles and delivers them to an unprotected exit. It is one of the primary failure modes for earth and rockfill embankment dams and accounts for roughly 50% of dam failures (Fell et al., 2015; Foster et al., 2000). Detection of internal erosion is difficult, if not impossible: as dams are tens of metres high and kilometres long, and erosion can occur at any location, it is challenging to be in the right place at the right time. The detection of internal erosion relies only on indicators: such as looking for seepage, checking the colour of the water and whether particles are removed with water during the routine visual monitoring, and monitoring the amount and rate of settlements by instruments. The more indicators we can use, the better we will be able to identify potential risks.

Fell et al. (2015) stated that long-term deformation monitoring is the most valuable data for detecting internal erosion and piping in the embankment dam, and the deformation data should be included in any

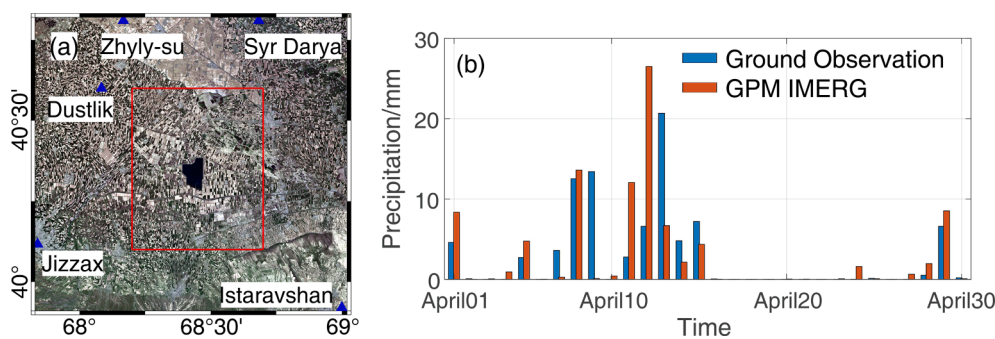


Fig. 11. Precipitation in April 2020 for the Sardoba Reservoir region. (a) The blue triangles are locations of nearby ground meteorological observations, and the red rectangle indicates the area for the Global Precipitation Measurement products. (b) The daily precipitation from ground observations (average of five stations) and the satellite products (average of the region).

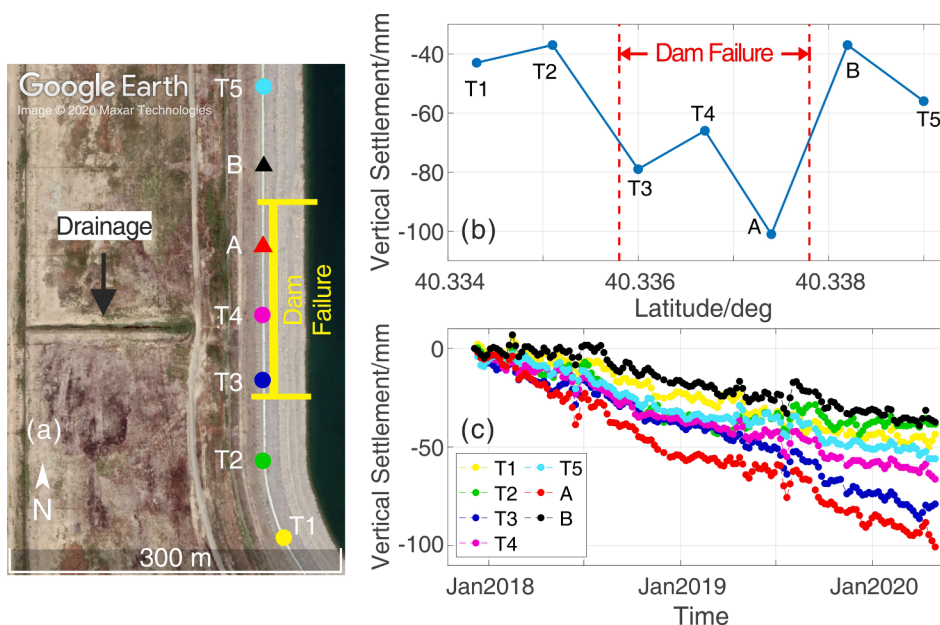


Fig. 12. The differential settlements near the Sardoba dam break section. (a) A closer look of the dam break section at satellite images from Google Earth™. T1 ~ T5, A and B show the locations of measurement points from SBAS InSAR. (b) Displacement profile along the embankment dam. (c) InSAR-derived settlement time series for locations T1 ~ T5, A and B.

dam safety review. The deformation results retrieved by InSAR with high accuracy, consistency, spatial and temporal resolution, is a reliable indicator for detecting internal erosion. In the case of Sardoba dam failure, the differential settlement phenomena at the dam break section before the event is the sign of internal erosion within the embankment. As the fill materials of the dam usually have low tensile strength, even small tensile stresses caused by uneven settlement may generate cracks where internal erosion initiates. The water retained behind the dam always tries to escape or flow along the path of the least resistance (Cedergren, 1973). Hydraulic fracturing further widens the cracks and leads to more uneven settlements. As the abnormal settlement of the embankment was left unattended (or more likely, it was not discovered before), the inside progressive erosion continued to develop without being appropriately remediated, which eventually caused the catastrophic consequence on the morning of 1 May 2020.

Internal erosion forms invisible waterways or pipes within a dam or its foundation and is always associated with the phenomenon of piping. Generally, internal erosion failures have three kinds of failure modes: internal erosion through the embankment, through the foundation, and from the embankment into the foundation. As cannot be observed directly, it is difficult to determine the exact location and mode of erosion damage. Historical statistics show that the percentage of internal erosion through embankment is twice that of erosion through the foundation, and more than 20 times as high as from the embankment into foundation (Foster et al., 2000). In the case of Sardoba, as no signal of uplift was detected near the dam toe, it is considered more likely that erosion occurs in the embankment rather than through the foundation.

Statistics show that about half of the internal erosion failures in embankments involved conduits embedded in the embankment dam. A flaw would most probably be formed where the soil is poorly compacted against conduits. Foster et al. (2000) and Fell et al. (2015) also concluded that for internal erosion failure mode, about two-thirds occurred on the first filling or in the first five years of operation, with almost all internal erosion failures through embankment occurring above or near the highest historical reservoir levels. As a drainage channel is seen near the failure section (Fig. 12a), the failure mode of internal erosion through the embankment related to the conduit is most compatible with the case of the Sardoba Reservoir dam collapse.

5.2. Why it happened: human factors

5.2.1. Human factors framework in dam failure investigations

The operation of the Sardoba Reservoir and the embankment dams involves interacting physical and human factors. Besides the physical factors, understanding the human factors that contribute to dam failure is an essential objective of the investigation. “Human factors” refer to beyond individual factors and include all group levels: organisations, industries, systems, etc. They consider how a system is performing and why it is not meeting expectations, with a focus on exploring causes and preventing incidents and failures (France et al., 2018). The human factors approaches have been widely used in the areas of aviation, nuclear power and chemical processing, etc. For civil infrastructure, the applications are more recent, with most of the works occurring in the last decade (Baker et al., 2020). Alvi (2013) introduced the “human factors framework” into the dam failure investigation, and it has been applied to the investigations of the 2004 Big Bay dam failure (Alvi, 2015), the 2017 Oroville spillway incident (France et al., 2018), and the 2019 Spencer dam failure (Baker et al., 2020).

According to the human factors framework and methodology, there are three types of deficiencies in risk management due to human errors: ignorance, complacency, and overconfidence. Ignorance is a lack of awareness of risk due to misunderstanding or lack of knowledge. Complacency is awareness of risk but being excessive in risk tolerance. Overconfidence involves the awareness of risks, but an overestimated ability to manage risk. The application of human factors framework presents a synthesis of various perspectives.

5.2.2. Ignorance of differential settlement: limited monitoring resolution

Without reviewing operation monitoring records and interviews with operators, it is difficult to conclude with certainty what categories of human factors were involved in the Sardoba dam failure. However, given the limitations of current dam monitoring methods, it is not difficult to surmise that the likelihood of ignorance in this case is high. More specifically, performance monitoring during the operation phase mainly includes instrumentation and visual monitoring. Unfortunately, deformation surveys are “falling out of favour” (ICOLD, 1988). Even when implemented, commonly used instrumental monitoring, such as settlement measurement which is a hard-data indicator of internal

erosion, is based on point-by-point observations. For example, following the requirements of the Design Code for Plain Reservoir Project (Ma et al., 2009) in Shandong, China, one deformation monitoring profile should be set up on the dam surface for every kilometre. The local differential settlement of the Sardoba Reservoir dam, which had developed for years before the failure near the breach, is possibly undetectable due to the insufficient monitoring sites. In these unfavourable circumstances, possible signs of the dam failure, such as abnormal seepage, piping, etc., could only be hoped to be found in visual inspections. Visual monitoring has shortcomings, including the inability to detect subtle changes at the site and being limited by engineers' experience, energy, sense of responsibility, etc. The COVID-19 epidemic has might also impacted on the on-site work in 2020.

5.3. Lesson learned: InSAR monitoring to reduce risk of ignorance

It is concerned that whether the failure has weakened the Sardoba Reservoir embankment dam structure and whether the dam can be recovered to function after repairs and modifications. An update to the current monitoring program or a new program should be developed to better understand the dam operational behaviour and reduce further risks. Compared with traditional deformation monitoring methods (mainly levelling and GNSS), InSAR has advantages as shown in Table 1.

InSAR's unique ability to "turn back time" provides accurate and reliable data to describe the historical deformation of a dam breach, regardless of whether traditional on-site monitoring has been carried out. It is the basis for investigating the causes of the catastrophic failure, guiding the repair and rehabilitation work. The high spatial and temporal resolution of InSAR can compensate for the shortcomings of traditional methods and reduce the ignorance factor in risk management. We recommend incorporating InSAR into the deformation monitoring program, and accuracy validation should also be performed. Fig. 13 shows a monitoring result example of the dam section and buildings near the outlet work of the Sardoba Reservoir.

The reservoir outlet works are vital appurtenant structures, which need attention during deformation monitoring. In Fig. 13a, T6 and T7 are located on the dam crest, and T8 is on the roof of the outlet gatehouse. The outlet structure (gatehouse) remains stable, and the cumulative net settlement is almost zero. The dam section near the outlet works has settled by ~100 mm in more than two years, and the time-series deformation demonstrates that the area was experiencing the primary consolidation settlement. Compared to the deformation process near the failure section shown in Fig. 12, we can see the noticeable difference: the cumulative settlement, as well as the deforming rate, are highly consistent at the monitoring points (T6, T7 and C). No differential settlement occurs on the embankment near the outlet works of the Sardoba Reservoir.

The objective of monitoring the dam performance during the

Table 1
Different methods of measuring embankment dam deformation.

	Levelling	GNSS	InSAR
Measurement dimension	1D: settlement	3D	1D: range changes; 2D: with multi-geometry
Accuracy ^a (mm)	<1	2–4 horizontal, 5–10 vertical	~5 line-of-sight
Temporal Resolution	Low: ~several months	High: up to seconds	Relatively high: up to days
Spatial Resolution	Low: pointwise and line-network	Low: pointwise and network	High: surface mapping
On-site work labour	High	Low	Rare
Cost ^b	High	High	Low considering monitoring scale

^a Under optimum conditions.

^b Including maintenance.

operation phase is twofold. To begin with, the owner/governor needs to ensure that the dam is behaving within the predetermined tolerable limits and that it is operating its design function safely. It relates to the human factors of ignorance in risk management. Moreover, as an essential issue in performance monitoring, the determination of the tolerable limits is based on past experiences of similar projects whose performances are considered acceptable. The monitoring results of existing dams help establish a judgement basis for future works (also for the modification of their tolerable limits). This contributes to reducing the risk of overconfidence. As Sentinel-1 and other upcoming satellite missions keep collecting Earth observations, it will be beneficial to establish a long-term InSAR deformation monitoring database of the Sardoba Reservoir dam with sufficient information density, high consistency and reliability. The advantages of InSAR resolution not only help reduce the risk of ignorance, but also provide the basis for enhancing engineering judgment in the form of more behavioural details.

6. Conclusions

The Sardoba Reservoir dam failure is a tragedy that caused casualties, environmental damages and economic losses. Investigation should avoid "hindsight bias" and focus on finding the contributing factors and preventing similar incidents from happening again. We investigate the failure event based on Earth observation data: satellite altimetry products, i.e., ICESat-2 data, are applied to characterise the topographic environment of the study area; Sentinel-1 SAR data with multi-geometry are used to retrieve the pre-failure deformation of the Sardoba Reservoir embankment dam; optical images from Sentinel-2 satellites and Global Precipitation Measurement products are also involved in exploring the environmental status before the failure. The analysis of the causes of the Sardoba dam failure in terms of physical and human factors led to the following conclusions:

- (1) The May 2020 Sardoba dam failure is a result of interactions of both physical and human factors. Based on the analysis of remote sensing data, it is considered that the physical factor contributing to the failure was internal erosion through the embankment, and the human factor of ignorance led to the loss of a possible opportunity to prevent the event. The differential settlement revealed by InSAR at the failure section before the event, which reached ~60 mm in two and a half years, should have been an indication of internal erosion. However, the unusual deformation pattern may not be undetected due to the resolution limitations of current dam monitoring methods.
- (2) Neither ground observations nor satellite-based Global Precipitation Measurement products recorded extreme rainfall in the region, so the possibility of overtopping due to rainfall-induced flood can be ruled out in the cause investigation.
- (3) InSAR results demonstrate that the maximum cumulative settlement occurred on the northern part of the dam, exceeding 120 mm between December 2017 and April 2020. It is inferred that the section has settled by ~270 mm since use, reaching ~0.8% of the dam height. Although the magnitude of deformation is not unusual, it should arouse close attention in the later stage.
- (4) InSAR time-series displacements indicate that the Sardoba Reservoir embankment dam is experiencing the primary consolidation settlement, and the settling rate does not present a remarkable decreasing trend with time. The deformation of the dam is dominated by consolidation settlement and partially influenced by fluctuations in reservoir water level.
- (5) The differential settlement developed years before the Sardoba dam failure is an indicator of internal erosion through the embankment, but had probably been ignored due to the limited resolution of conventional deformation monitoring methods. InSAR captures the pre-failure deformation signals well,

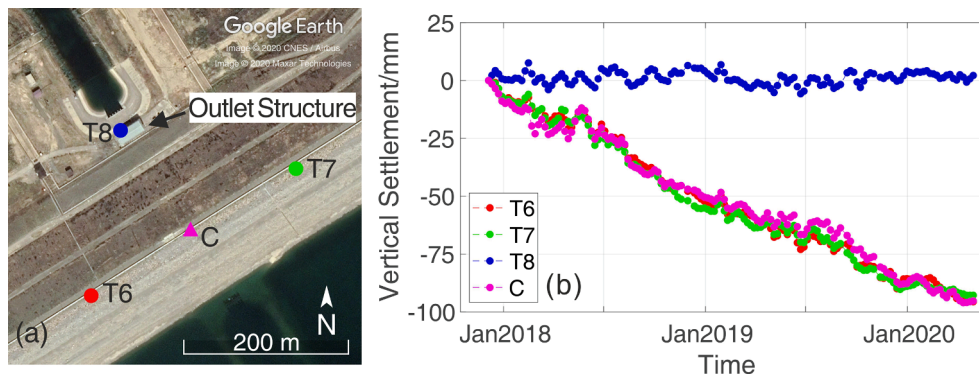


Fig. 13. An example of the settlement monitoring result by InSAR. (a) A closer look of the Sardoba Reservoir outlet works at satellite images from Google Earth™. T6 ~ T8 and C show the locations of measurement points from InSAR. (b) Monitoring results (vertical deformation time series) from December 2017 to April 2020 derived from InSAR measurements.

suggesting that early warning of risks is possible and that the Sardoba dam failure could have been avoided with appropriate intervention. We recommend InSAR deformation monitoring be included in future safety programs to provide detailed deformation and reduce risks of ignorance.

CRedit authorship contribution statement

Ruya Xiao: Conceptualization, Methodology, Investigation, Writing – original draft. **Mi Jiang:** Methodology, Writing – review & editing. **Zhenhong Li:** Conceptualization, Supervision, Writing – review & editing. **Xiufeng He:** Funding acquisition.

Declaration of Competing Interest

The authors declare that they have no known competing financial interests or personal relationships that could have appeared to influence the work reported in this paper.

Acknowledgements

This research was supported by the National Natural Science Foundation of China (grant numbers 42174018, 41804005, 41941019, 41830110); the Fundamental Research Funds for the Central Universities (grant number B210202111); the Open Foundation of Key Lab of Reservoir Dam Safety of the Ministry of Water Resources, China (grant number YK321008). The authors thank the European Space Agency for providing the Sentinel-1&2 images, NASA for the ICESat-2 data, and NASA/JAXA for providing the Global Precipitation Measurement products.

References

- Al-Husseinawi, Y., Li, Z., Clarke, P., Edwards, S., 2018. Evaluation of the stability of the Darbandikhan dam after the 12 November 2017 Mw 7.3 Sarpol-e Zahab (Iran-Iraq Border) earthquake. *Remote Sens.* 10. <https://doi.org/10.3390/rs10091426>.
- Alvi, I.A., 2015. Human factors contributing to failure of Big Bay Dam [WWW Document]. URL https://www.researchgate.net/publication/286074653_Human_factors_contributing_to_failure_of_Big_Bay_Dam (accessed 1.1.21).
- Alvi, I.A., 2013. Human factors in dam failures. In: 2013 Dam Safety Conference Proceedings. Association of State Dam Safety Officials, Rhode Island, USA.
- ASCE, 2017. 2017 Infrastructure report card: A comprehensive assessment of America's infrastructure. Reston, Virginia, USA. https://doi.org/10.1007/978-3-319-13296-9_12.
- ASDSO, 2020. Dam Failures and Incidents [WWW Document]. URL <https://damsafety.org/dam-failures> (accessed 9.1.20).
- Baker, M.E., Ettema, R., Teal, M., Trojanowski, J., 2020. Association of State Dam Safety Officials: Spencer Dam failure investigation report. Lexington, Kentucky, USA.
- BBC News, 2020. Michigan floods: Evacuations after Edenville and Sanford dams breached [WWW Document]. URL <https://www.bbc.co.uk/news/world-us-canada-52735170#> (accessed 9.1.20).

- Biggs, J., Wright, T.J., 2020. How satellite InSAR has grown from opportunistic science to routine monitoring over the last decade. *Nat. Commun.* 11 (1) <https://doi.org/10.1038/s41467-020-17587-6>.
- Cedergren, H.R., 1973. Seepage control in earth dams. In: Hirschfeld, R.C., Poulos, S.J., Bertram, G.E. (Eds.), *Embankment Dam Engineering: Casagrande Volume*. Wiley, New York USA.
- Chang, L., Hanssen, R.F., 2014. Detection of cavity migration and sinkhole risk using radar interferometric time series. *Remote Sens. Environ.* 147, 56–64. <https://doi.org/10.1016/j.rse.2014.03.002>.
- Chen, C.W., Zebker, H.A., 2002. Phase unwrapping for large SAR interferograms: statistical segmentation and generalized network models. *IEEE Trans. Geosci. Remote Sens.* 40 (8), 1709–1719. <https://doi.org/10.1109/TGRS.2002.802453>.
- Cigna, F., Tapete, D., 2021a. Present-day land subsidence rates, surface faulting hazard and risk in Mexico City with 2014–2020 Sentinel-1 IW InSAR. *Remote Sens. Environ.* 253, 112161. <https://doi.org/10.1016/j.rse.2020.112161>.
- Cigna, F., Tapete, D., 2021b. Satellite InSAR survey of structurally-controlled land subsidence due to groundwater exploitation in the Aguascalientes Valley, Mexico. *Remote Sens. Environ.* 254, 112254. <https://doi.org/10.1016/j.rse.2020.112254>.
- CSSTEAP, 2020. Centre for Space Science and Technology Education in Asia and the Pacific (CSSTEAP) analyses Sardoba dam failure [WWW Document]. URL <http://www.un-spider.org/news-and-events/news/cssteap-analyses-sardoba-dam-failure> (accessed 8.31.20).
- D'Amico, F., Gagliardi, V., Bianchini Ciampoli, L., Tosti, F., 2020. Integration of InSAR and GPR techniques for monitoring transition areas in railway bridges. *NDT and E Int.* 115, 102291. <https://doi.org/10.1016/j.ndteint.2020.102291>.
- Dini, B., Manconi, A., Loew, S., Chopel, J., 2020. The Punatsangchu-I dam landslide illuminated by InSAR multitemporal analyses. *Sci. Rep.* 10, 1–10. <https://doi.org/10.1038/s41598-020-65192-w>.
- Du, Z., Ge, L., Ng, A.-M., Zhu, Q., Horgan, F.G., Zhang, Q.i., 2020. Risk assessment for tailings dams in Brumadinho of Brazil using InSAR time series approach. *Sci. Total Environ.* 717, 137125. <https://doi.org/10.1016/j.scitotenv.2020.137125>.
- Emadali, L., Motagh, M., Haghshenas Haghghi, M., 2017. Characterizing post-construction settlement of the Masjed-Soleyman embankment dam, Southwest Iran, using TerraSAR-X SpotLight radar imagery. *Eng. Struct.* 143, 261–273. <https://doi.org/10.1016/j.engstruct.2017.04.009>.
- Fell, R., MacGregor, P., Stapledon, D., Bell, G., Foster, M., 2015. *Geotechnical Engineering of Dams*, 2nd ed. CRC Press/Balkema, EH Leiden, The Netherlands.
- Ferretti, A., Prati, C., Rocca, F., 2001. Permanent scatterers in SAR interferometry. *IEEE Trans. Geosci. Remote Sens.* 39, 8–20. <https://doi.org/10.1109/36.898661>.
- Fornós, J., Arroyo, M., Guerra, J., Conde, A., Salva, B., Garcia, M., 2017. The use of InSAR data to monitor slope stability of dams and water reservoirs. In: The 85th Annual Meeting of International Commission on Large Dams. Prague, Czech Republic.
- Foster, M., Fell, R., Spannagle, M., 2000. The statistics of embankment dam failures and accidents. *Can. Geotech. J.* 37 (5), 1000–1024. <https://doi.org/10.1139/t00-030>.
- France, J.W., Alvi, I.A., Dickson, P.A., Falvey, H.T., Rigby, S.J., Trojanowski, J., 2018. Independent Forensic Team Report: Oroville Dam Spillway Incident [WWW Document]. URL <https://damsafety.org/sites/default/files/files/Independent%20Forensic%20Team%20Report%20Final%20001-05-18.pdf> (accessed 1.1.21).
- Fuhrmann, T., Garthwaite, M.C., 2019. Resolving three-dimensional surface motion with InSAR: Constraints from multi-geometry data fusion. *Remote Sens.* 11, 241. <https://doi.org/10.3390/rs11030241>.
- Giri, S., Donchyts, G., Hegnauer, M., 2020. Rapid desk analysis of the dam breach at Sardoba reservoir in Uzbekistan [WWW Document]. URL https://www.researchgate.net/publication/341326590_Rapid_desk_analysis_of_the_dam_breach_at_Sardoba_reservoir_in_Uzbekistan (accessed 1.1.21).
- Grebby, S., Sowter, A., Gluyas, J., Toll, D., Gee, D., Athab, A., Girindran, R., 2021. Advanced analysis of satellite data reveals ground deformation precursors to the Brumadinho Tailings Dam collapse. *Commun. Earth Environ.* 2, 1–9. <https://doi.org/10.1038/s43247-020-00079-2>.
- Haghshenas Haghghi, M., Motagh, M., 2019. Ground surface response to continuous compaction of aquifer system in Tehran, Iran: Results from a long-term multi-sensor

- InSAR analysis. *Remote Sens. Environ.* 221, 534–550. <https://doi.org/10.1016/j.rse.2018.11.003>.
- Hooper, A., Segall, P., Zebker, H., 2007. Persistent scatterer interferometric synthetic aperture radar for crustal deformation analysis, with application to Volcán Alcedo, Galápagos. *J. Geophys. Res. Solid Earth* 112 (B7). <https://doi.org/10.1029/2006JB004763>.
- Hu, X., Ommen, T., Lu, Z., Wang, T., Kim, J.W., 2017. Consolidation settlement of Salt Lake County tailings impoundment revealed by time-series InSAR observations from multiple radar satellites. *Remote Sens. Environ.* 202, 199–209. <https://doi.org/10.1016/j.rse.2017.05.023>.
- Huffman, G.J., Bolvin, D.T., Braithwaite, D., Hsu, K.L., Joyce, R.J., Kidd, C., Nelkin, E.J., Sorooshian, S., Stocker, E.F., Tan, J., Wolff, D.B., Xie, P., 2020. Integrated Multi-satellite Retrievals for the Global Precipitation Measurement (GPM) Mission (IMERG). In: *Advances in Global Change Research*. Springer, pp. 343–353. https://doi.org/10.1007/978-3-030-24568-9_19.
- ICOLD, 1988. The International Commission on Large Dams: Dam monitoring - General considerations. Paris, France.
- Jiang, M., 2020. Sentinel-1 TOPS co-registration over low-coherence areas and its application to velocity estimation using the all pairs shortest path algorithm. *J. Geod.* 94, 1–15. <https://doi.org/10.1007/s00190-020-01432-1>.
- Liu, P., Li, Z., Hoey, T., Kincal, C., Zhang, J., Zeng, Q., Muller, J.-P., 2013. Using advanced InSAR time series techniques to monitor landslide movements in Badong of the Three Gorges region, China. *Int. J. Appl. Earth Obs. Geoinf.* 21, 253–264. <https://doi.org/10.1016/j.jag.2011.10.010>.
- Lu, Z., Dzurisin, D., Lu, Z., Dzurisin, D., 2014. InSAR Imaging of Aleutian Volcanoes. In: *InSAR Imaging of Aleutian Volcanoes*. Springer, Berlin Heidelberg, pp. 87–345. https://doi.org/10.1007/978-3-642-00348-6_6.
- Ma, C., Wang, L., Xu, Y., Dai, T., Ke, H., Miao, J., Lin, R., Duan, D., Gao, F., Zhu, Z., Zheng, D., Wu, C., Zhou, R., Liu, H., Jin, R., 2009. Design Code for Plain Reservoir Project (Shandong Provincial Standard DB37/1342-2009), 1st ed. China Water Conservancy and Hydropower Press.
- Martire, Diego Di, Iglesias, R., Monells, D., Centolanza, G., Sica, S., Ramondini, M., Pagano, L., Mallorquí, J.J., Calaterra, D., 2014. Comparison between Differential SAR interferometry and ground measurements data in the displacement monitoring of the earth-dam of Conza della Campania (Italy). *Remote Sens. Environ.* 148, 58–69. <https://doi.org/10.1016/j.rse.2014.03.014>.
- Milillo, P., Bürgmann, R., Lundgren, P., Salzer, J., Perissin, D., Fielding, E., Biondi, F., Milillo, G., 2016a. Space geodetic monitoring of engineered structures: The ongoing destabilization of the Mosul dam, Iraq. *Sci. Rep.* 6, 1–7. <https://doi.org/10.1038/srep37408>.
- Milillo, P., Perissin, D., Salzer, J.T., Lundgren, P., Lacava, G., Milillo, G., Serio, C., 2016b. Monitoring dam structural health from space: Insights from novel InSAR techniques and multi-parametric modeling applied to the Pertusillo dam Basilicata, Italy. *Int. J. Appl. Earth Obs. Geoinf.* 52, 221–229. <https://doi.org/10.1016/j.jag.2016.06.013>.
- Ministry of Water Resources P.R.China and National Bureau of Statistics P.R.China, 2013. Bulletin of first national census for water. Beijing, China.
- NASA Earth Observatory, 2020. NASA Earth Observatory: Flooding in Uzbekistan and Kazakhstan [WWW Document]. URL <https://earthobservatory.nasa.gov/images/146703/flooding-in-uzbekistan-and-kazakhstan> (accessed 8.31.20).
- Neuenschwander, A.L., Popescu, S.C., Nelson, R.F., Harding, D., Pitts, K.L., Robbins, J., 2019. ATLAS/ICESat-2 L3A Land and Vegetation Height, Version 2 [WWW Document]. Boulder, Colorado USA. NSIDC: National Snow and Ice Data Center. <https://doi.org/10.5067/ATLAS/ATL08.002>.
- Saleh, M., Masson, F., Mohamed, A.M.S., Boy, J.P., Abou-Aly, N., Rayan, A., 2018. Recent ground deformation around lake Nasser using GPS and InSAR, Aswan. *Egypt. Tectonophys.* 744, 310–321. <https://doi.org/10.1016/j.tecto.2018.07.005>.
- Silva Rotta, L.H., Alcántara, E., Park, E., Negri, R.G., Lin, Y.N., Bernardo, N., Mendes, T.S.G., Souza Filho, C.R., 2020. The 2019 Brumadinho tailings dam collapse: Possible cause and impacts of the worst human and environmental disaster in Brazil. *Int. J. Appl. Earth Obs. Geoinf.* 90, 102119. <https://doi.org/10.1016/j.jag.2020.102119>.
- The Economist, 2020. A dam failure raises concerns about corruption in Uzbekistan [WWW Document]. The Economist. URL <https://www.economist.com/asia/2020/08/08/a-dam-failure-raises-concerns-about-corruption-in-uzbekistan> (accessed 8.31.20).
- Tomás, R., Cano, M., García-Barba, J., Vicente, F., Herrera, G., Lopez-Sanchez, J.M., Mallorquí, J.J., 2013. Monitoring an earthfill dam using differential SAR interferometry: La Pedrera dam, Alicante, Spain. *Eng. Geol.* 157, 21–32. <https://doi.org/10.1016/j.enggeo.2013.01.022>.
- U.S. Department of the Interior Bureau of Reclamation, 2011. Design Standards No. 13 Embankment Dams -Chapter 9: Static Deformation Analysis Phase 4 (Final), DS-13 (9)-1. ed. Denver, Colorado, USA.
- U.S. Department of the Interior Bureau of Reclamation, 1987. Design of Small Dams, third ed. United States Government Publishing Office, Denver, Colorado, USA.
- Wang, Q.Q., Huang, Q.H., He, N., He, B., Wang, Z.C., Wang, Y.A., 2020. Displacement monitoring of upper Atbara dam based on time series InSAR. *Surv. Rev.* 52 (375), 485–496. <https://doi.org/10.1080/00396265.2019.1643529>.
- Wang, T., Perissin, D., Rocca, F., Liao, M.-S., 2011. Three Gorges Dam stability monitoring with time-series InSAR image analysis. *Sci. China Earth Sci.* 54 (5), 720–732. <https://doi.org/10.1007/s11430-010-4101-1>.
- Wang, T., Shi, Q., Nikkhoo, M., Wei, S., Barbot, S., Dreger, D., Bürgmann, R., Motagh, M., Chen, Q.F., 2018. The rise, collapse, and compaction of Mt. Mantap from the 3 September 2017 North Korean nuclear test. *Science* 361, 166–170. <https://doi.org/10.1126/science.aar7230>.
- Wright, T.J., Parsons, B.E., Lu, Z., 2004. Toward mapping surface deformation in three dimensions using InSAR. *Geophys. Res. Lett.* 31 <https://doi.org/10.1029/2003GL018827>.
- Wu, S., Yang, Z., Ding, X., Zhang, B., Zhang, L., Lu, Z., 2020. Two decades of settlement of Hong Kong International Airport measured with multi-temporal InSAR. *Remote Sens. Environ.* 248, 111976. <https://doi.org/10.1016/j.rse.2020.111976>.
- Xi, R., Zhou, X., Jiang, W., Chen, Q., 2018. Simultaneous estimation of dam displacements and reservoir level variation from GPS measurements. *Measurement* 122, 247–256. <https://doi.org/10.1016/j.measurement.2018.03.036>.
- Xiao, R., He, X., 2019. Deformation Monitoring of Reservoirs and Dams Using Time-Series InSAR. *Geomatics and Information Science of Wuhan University* 44. <https://doi.org/10.13203/j.whugis20170327>.
- Xiao, R., Shi, H., He, X., Li, Z., Jia, D., Yang, Z., 2019. Deformation Monitoring of Reservoir Dams Using GNSS: An Application to South-to-North Water Diversion Project, China. *IEEE Access* 7, 54981–54992. <https://doi.org/10.1109/ACCESS.2019.2912143>.
- Xu, X., Sandwell, D.T., 2020. Toward Absolute Phase Change Recovery With InSAR: Correcting for Earth Tides and Phase Unwrapping Ambiguities. *IEEE Trans. Geosci. Remote Sens.* 58 (1), 726–733. <https://doi.org/10.1109/TGRS.2019.2940207>.
- Zhang, JianYun, Yang, ZhengHua, Jiang, JinPing, 2017. An analysis on laws of reservoir dam defects and breaches in China. *SCIENTIA SINICA Technologica* 47 (12), 1313–1320. <https://doi.org/10.1360/N092016-00295>.
- Zhang, J., Yang, Z., Jiang, J., 2014. A study on Reservoir dam defects and breaches in China, 1st ed. Science Press, Beijing, China.
- Zhou, W., Li, S., Zhou, Z., Chang, X., 2016. Remote sensing of deformation of a high concrete-faced rockfill dam using InSAR: A study of the Shuibuya dam, China. *Remote Sens.* 8, 255. <https://doi.org/10.3390/rs8030255>.